PAPER

A triboelectric nanogenerator based on food packaging Aluminium foil and Parafilm for self-powered electronics

Physica Scripta

PAPER

A triboelectric nanogenerator based on food packaging Aluminium foil and Parafilm for self-powered electronics

P Ravi Sankar[1], K Prakash[1,*], P Supraja[2], R Rakesh Kumar[2,†,*], Siju Mishra[2] and D Haranath[2]

[1] Department of Electronics and Communication Engineering, Flexible Electronics Lab, National Institute of Technology-Warangal, 506004, India
[2] Department of Physics, Energy Materials and Devices Lab, National Institute of Technology-Warangal, 506004, India
[†] https://sites.google.com/site/rakeshrajaboina/
[*] Authors to whom any correspondence should be addressed.

E-mail: kprakash@nitw.ac.in **and** rakeshr@nitw.ac.in

RECEIVED
7 June 2021

REVISED
18 August 2021

ACCEPTED FOR PUBLICATION
24 August 2021

PUBLISHED
6 September 2021

Keywords: triboelectric nanogenerators, Parafilm, energy harvesting, self-powered electronics, waste food packaging Aluminium covers

Supplementary material for this article is available online

Abstract

The increasing food packaging waste is a severe concern for air, water, and soil pollution. In this research work, a triboelectric nanogenerator (TENG) is fabricated using waste food packaging Aluminium cover foils and laboratory parafilm for the first time. The device novelty lies in the selection of the materials; parafilm and food packing Aluminium cover foils. The proposed TENG produced an output voltage and instantaneous power density of ~4 V and 11.8 nW cm^{-2}, respectively, by hand excitation force. Further, TENG can easily power up 85 commercial light-emitting diodes, digital watch, thermometer, and calculator with the help of charged capacitor. The proposed TENG demonstrated the ease of process, simplicity, cost-effectiveness, and reduction of pollution. Further, this TENG performance can be improved with other triboelectric materials and applied in self-powered portable electronic device applications.

1. Introduction

Triboelectric nanogenerators (TENG) have attracted increased attention due to their multifunctional applications in various fields such as bio-medical, healthcare, Internet of things, artificial intelligence, and self-powered electronic devices and sensors [1–6]. The first TENG was reported in 2012 and developed to effectively convert ambient mechanical energy, such as body motion, wind, and vibration energy into electrical energy [2, 7]. The typical TENG consists of two different electronegativity layers. These layers generate potential difference via the coupling of the triboelectric effect and electrostatic induction during cyclic contact and separation between them [8, 9]. Subsequently, TENG has AC to DC conversion circuits, storage elements such as a battery or capacitor to power up portable electronic devices or sensors [10, 11]. Four different modes of TENG operation have been proposed based on electrode configuration and direction of polarization change. These four modes are vertical contact-separation, lateral-sliding, single-electrode, and free-standing triboelectric layer [12, 13]. The contact separation mode is very well established among different modes and demonstrated for many triboelectric materials [14, 15]. In the present manuscript, also vertical contact separation mode of TENG operation is used. The main advantages of TENGs are their high energy-conversion efficiency, simple structure, cost-effectiveness, reliability, scalability, and harvesting energy from irregular, low-frequency inputs [16, 17]. A wide variety of triboelectric pairs tested for energy harvesting and demonstrated for potential practical applications are summarized in figure 1 [18, 19].

However, the search for new triboelectric materials is still considered an important area of research to reduce the TENG device's cost and complexity and improve its energy conversion efficiency. There are various triboelectric materials such as inorganic, organic, polymer, and bio-waste materials [19–22]. The energy generation from waste attracted much attention due to the reduction of pollution in the environment. Many

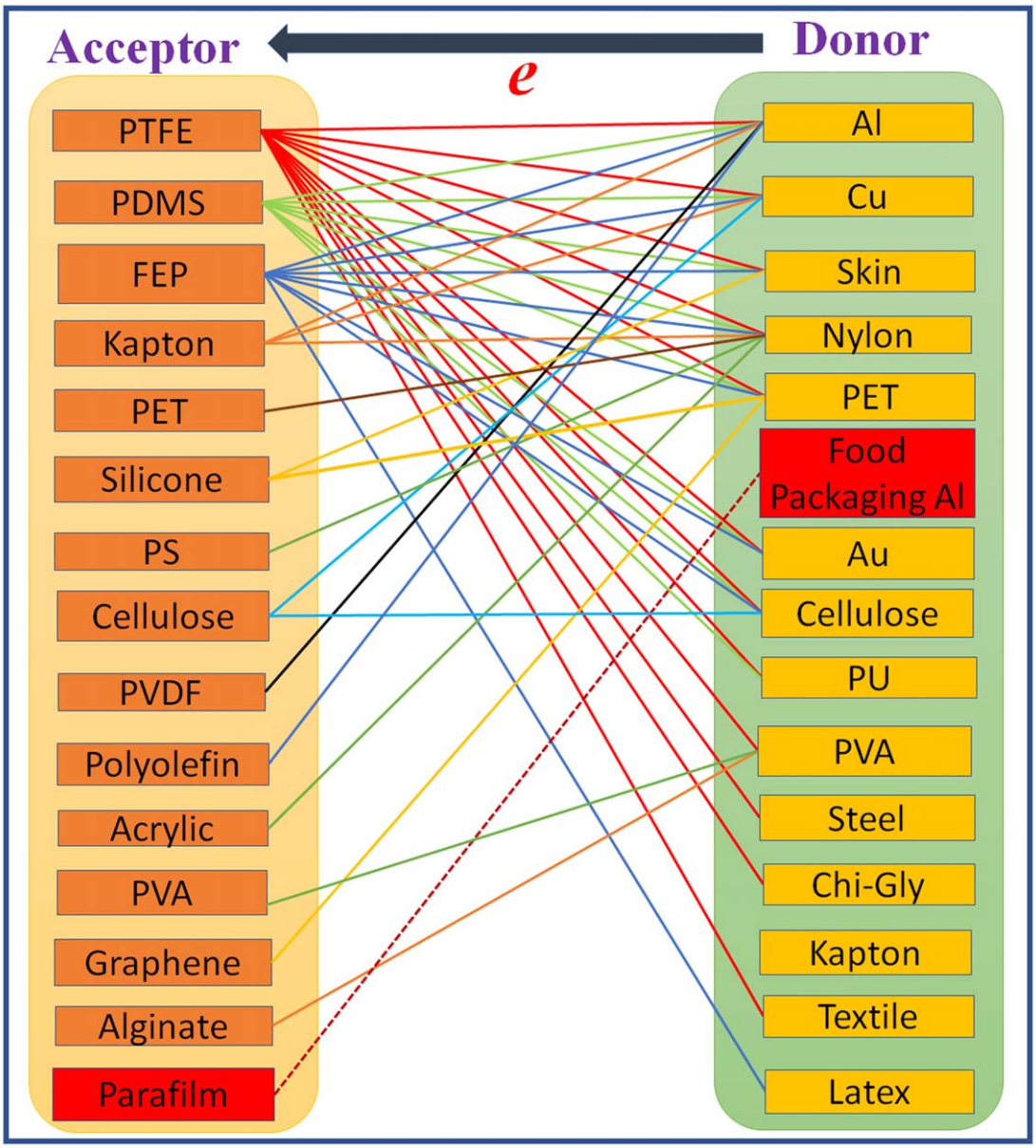

Figure 1. List of triboelectric pairs reported in the literature and our current work highlighted in dotted line [19].

recent reports are dealing with the new triboelectric materials from the waste materials for energy harvesting applications. J Bae *et al* reported the biowaste Peanut shell powder, Sunflower husks powder based TENG for biomechanical energy harvesting [23, 24]. J M Wu *et al* demonstrated high current density TENG based on rice husk [25]. Z Zhu *et al* developed TENG based on waste tea leaves and waste aluminium plastic bags [26].

Z L Wang *et al* demonstrated a novel TENG based on the waste milk carton and used for *in situ* real-time survey of environmental monitoring [27, 28]. H Singh *et al* fabricated TENG using an eggshell membrane with other triboelectric materials and demonstrated for powering the digital watch [29]. P Zhang *et al* used recycled PVC cling film as a triboelectric layer and used it for Morse code generation [30]. G Han *et al* fabricated the TENG based on waste plastic bags [31]. It is found that output voltage of waste material based TENG's in the range of 6–600 volts and power density in the range of 0.25 μW m^{-2}–0.84 W m^{-2} (See supplementary information (SI) S1 (available online at stacks.iop.org/PS/96/125005/mmedia)). In this manuscript, waste food packing Aluminium cover (WFPAC) foil and laboratory parafilm were used as a new triboelectric pair for mechanical energy harvesting for the first time. Parafilm is a semi-transparent, flexible film composed of a proprietary blend of waxes and polyolefins. It has several advantages: flexible, moldable, self-sealing, odourless, moisture-resistant, thermoplastic, semi-transparent, and colorless. The WFPAC is a polymer (PET) film electroplated with Aluminium. The reuse of WFPAC foils for energy harvesting strongly promotes the

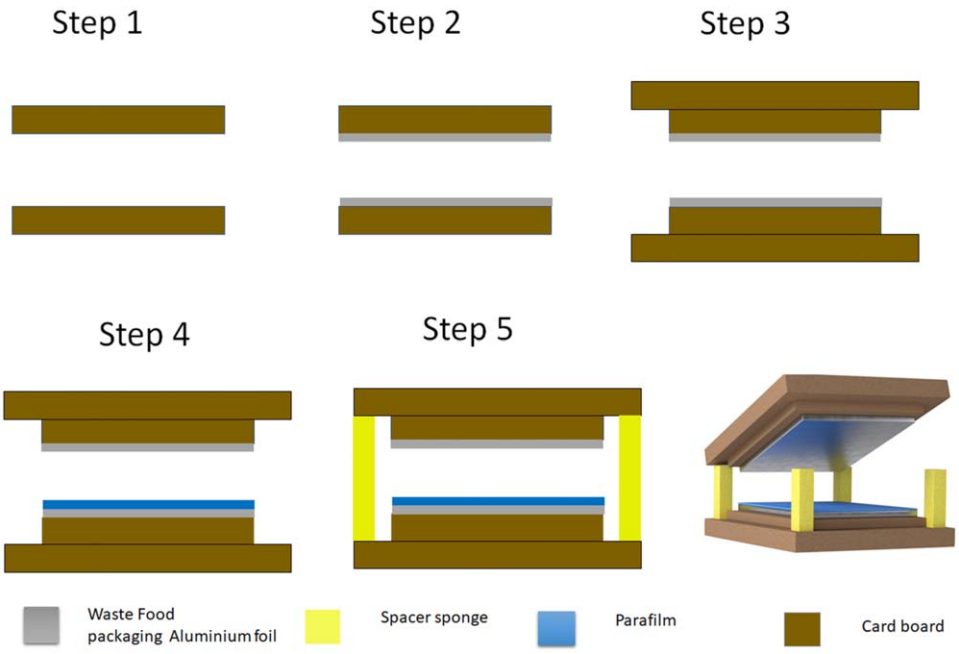

Figure 2. Fabrication steps of TENG based on parafilm and waste food packaging aluminium foil.

next-generation energy technologies that will effectively avoid pollution and hazards caused by metal and hardly degradable plastic materials.

In this report, a novel TENG is fabricated based on WFPAC foil and parafilm for mechanical energy harvesting for the first time and studied its performance. Further, fabricated TENG has been demonstrated to power up portable electronic devices and a group of LEDs.

2. Materials and methods

The materials used in this study are cardboard sheets, WFPAC foils, laboratory parafilm, and sponge. The Parafilm-M was purchased from Sigma Aldrich. The Aluminium packaging foils, cardboards, sponges were obtained from the local market (See SI, S2). The obtained Aluminium foils were used for cooked rice packaging initially and then used for TENG. The Parafilm and WFPAC foils are initially characterized by a scanning electron microscope (SEM). Then, TENG was fabricated using parafilm (thickness ~180 μm) and WFPAC foil (thickness ~35 μm), cardboard sheets, and sponge spacers. The fabrication steps of the TENG are shown in figure 2.

Initially, WFPAC attached to two rigid cardboards of selected dimension firmly by scotch tape with conducting side up. Further, parafilm is firmly attached to one of the above structures on the conductive side with scotch tape. These two cardboards with electrodes and parafilm were attached to another two cardboard sheets of higher dimension than this with a spacer. Four corners of the bottom cardboard were attached with sponge spacers with the help of strong glue. Another cardboard with only WFPAC foil is placed over the spacer and attached with the help of the strong glue. A finite gap exists between the bottom parafilm and the top Aluminium electrode due to the sponge spacer. The original images of the fabricated TENG devices and fabrication steps are shown in figure 3.

Generally, TENG devices work in four modes: vertical contact separation, in-plane sliding, single-electrode, and free-standing triboelectric-layer [2]. In this work, TENGs were designed to operate in the vertical contact mode. At open-circuit conditions, the charge generation of the TENG under cyclic force application can be understood from the coupling of the triboelectric effect and electrostatic induction [2]. Figure 4 schematically presents the working mechanism of the TENG with parafilm under the vertical compressive force. The mechanism is well-reported and accepted in the literature [2, 8].

In the initial state, before the contact of the parafilm and the top Aluminium electrode, there is no charge transfer and thus no electric potential, like shown in figure 4(a). As shown in figure 4(b), when parafilm and Aluminium contact each other, exchange of charges between Aluminium and parafilm due to their different abilities to gain or lose charge. The parafilm carries a negative charge while Aluminium carries the same amount of positive charge, keeping the TENG in a balanced state. When the TENG starts to separate, the balance is

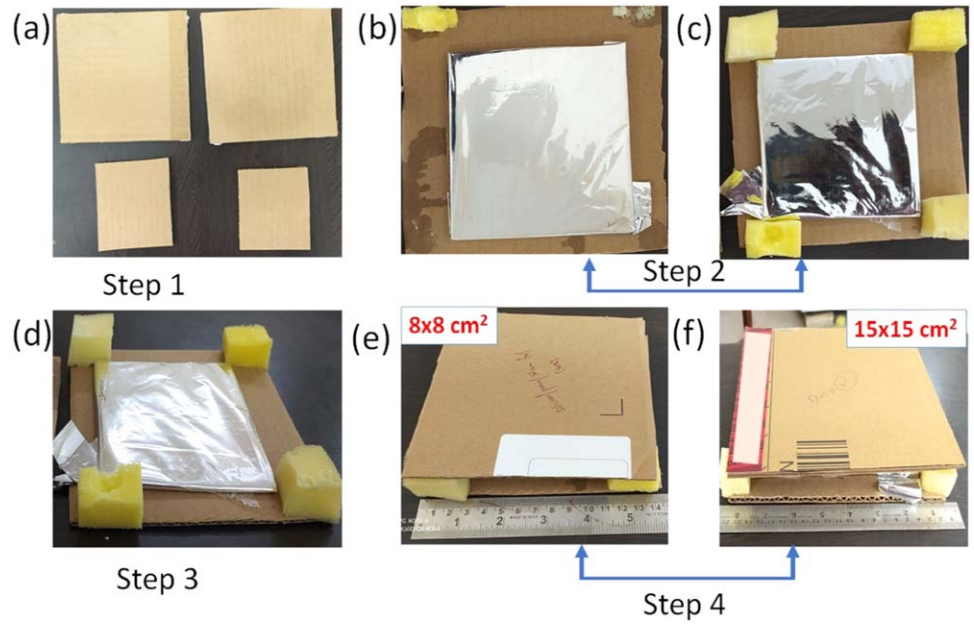

Figure 3. Photographs of TENG's fabrication steps based on parafilm and waste food packaging Aluminium foil (a) cardboard sheets for upper (large) and inner (small) parts of the TENG, (b)–(c) aluminium foil attached to inner cardboard sheets, (d) parafilm attached to the aluminium foil of figures (c), (e), (f) packed 8 × 8 and 15 × 15 cm^2 TENG device.

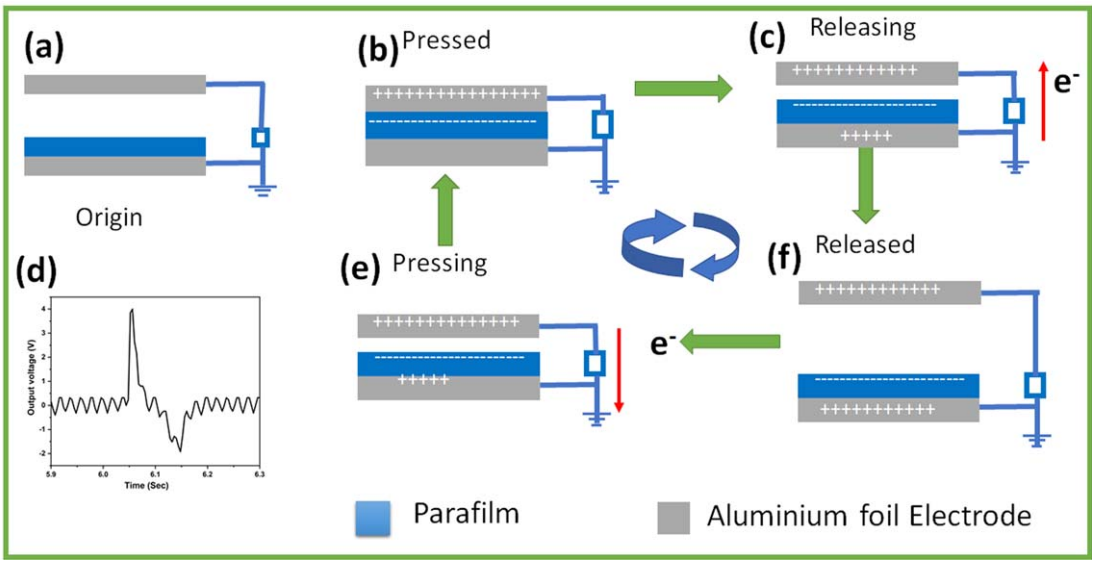

Figure 4. (a)–(c), (e), (f) working mechanism of TENG, (d) press and release signal output voltage pulse.

broken due to the electrical potential difference. The parafilm can retain charges on its surface, which remains unchanged, so a balanced state is rebuilt. The charges on the electrode surface will transfer from the parafilm electrode to the Aluminium, as shown in figures 4(c), (f). When the two surfaces are brought together again (figure 4(e)), the electrical balance is broken and rebuilt again. In this state, charges transfer from Aluminium to the parafilm electrode until the balance is reached (figure 4(b)). During the periodical contact-separation process, the triboelectric charges on the parafilm induce a periodical movement of the free electrons on the top and bottom Aluminium electrodes to generate electron flows in the external circuit.

The TENGs were prepared with a different active area of 5 × 5, 8 × 8, 15 × 15 cm^2 for a fixed spacing of 1.5 cm between the parafilm and WFPAC foil using the exact dimension spacer. Further, TENGs were fabricated with different spacer dimensions for a fixed active area of the device (15 × 15 cm^2) to study the spacer size. Finally, fabricated TENG output voltage against hand tapping was measured using a digital storage oscilloscope (Tektronix-TBS1102) interfaced to a computer using the software as reported in the literature [32, 33].

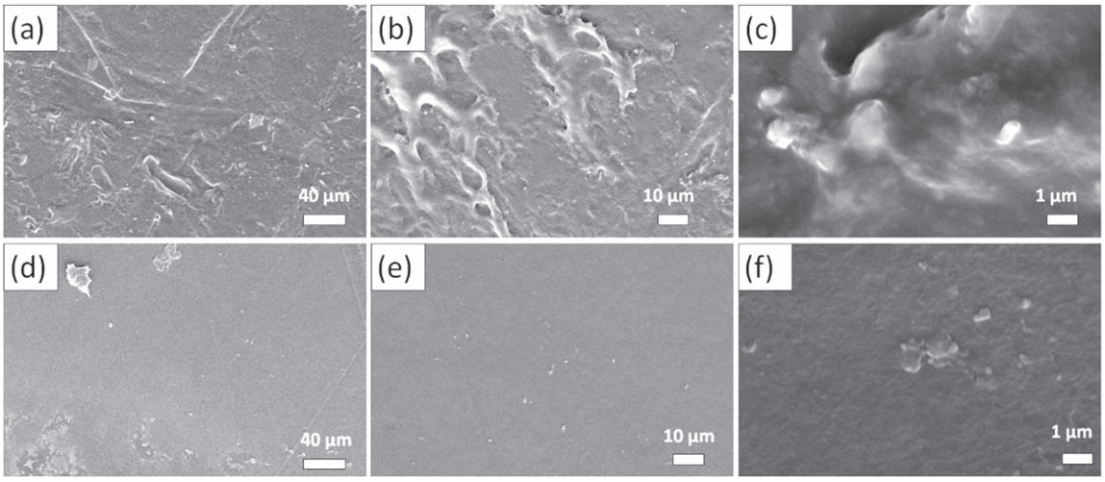

Figure 5. SEM images of the (a)–(c) parafilm, (d)–(f) aluminium packaging foil at different magnifications.

3. Results and discussion

Initially, the surface morphology of the parafilm and Aluminium foil was characterized with a scanning electron microscope. Figures 5(a)–(c) and (d)–(f) shows the SEM images of parafilm and Aluminium foil surface at different magnifications. It is clear from the SEM images that, parafilm films has rougher surface compared to Aluminium foil surface.

Figure 6(b) shows the open-circuit voltage of the $15 \times 15\ cm^2$ TENG (spacing $= 1.5$ cm) in response to the repeated hand tapping. An output voltage of ~4 V was observed for repeated hand tapping. A switching polarity test was performed by reversing the TENG connections to the oscilloscope to confirm the output voltage only due to TENG operation. The TENG has shown exactly opposite electrical signal in reverse connection with respect to the forward signal, as shown in figure 6(b). The switching polarity test confirms that the voltage generated is only from TENG, not from the instrument noise [7, 34]. The enlarged view of the single cycle (press and release) output voltage signal is shown in figure 6(c). We have also tested the output response of the TENG fabricated with fresh Aluminium foil -parafilm against hand tapping. It was found that no difference in their output voltage response when compared to the used Aluminium foil-based TENG. A similar output for both types of foil is due to the no abnormal changes on the surface at the microscopic level for the used foil (See SI, S3).

Further, TENG output voltage was measured with variable load resistances ranging from 20 KΩ to 100 MΩ under uniform hand tapping to measure the optimum output power density. The variation of output voltage under different load resistances is shown in figure 6(d). With an increase in load resistance, the voltage increases and saturates at a value of approximately ~3.8 V. The saturated output voltage at higher resistance (100 MΩ) is close to the open circuit output voltage. The TENG load resistance-dependent output voltage shows a similar trend as reported in the literature [35–37]. The TENG load resistance can be understood with the help of a simple equivalent model proposed by Z L Wang and other research groups in the literature [38, 39]. The TENG is equivalent to a variable capacitor connected to a voltage source. The voltage drops across the R_L increase until the optimum R_L and saturate at the theoretically infinite load resistance similar to open-circuit voltage [40].

The output power density (Power density $= \frac{V^2}{(A * R_L)}$) with different load resistances was calculated and summarized in figure 6(e). Figure 6(e) shows that the maximum output power density of the TENG is 11.8 nW cm^{-2}, at a load resistance of 1.8 MΩ. The output power density characteristics of the TENG device can be explained with the help of the maximum power transmission theorem [41]. According to the theorem, maximum power transmission takes place when the load resistance value equals to the source internal resistance. In the present report, the peak output power density occurred under impendence matched conditions across a load resistor value ~1.8 MΩ. The output power density decreased with the load resistance values greater than 1.8 MΩ due to the saturated output voltage. The saturated output voltage at higher load resistance decreases the V^2/R_L ratio (power) value. The output power density of TENG with load resistance shows a similar trend as reported in the literature [28, 32, 42]. Figure 6(f) shows the rectified output voltage of the TENG after rectification via DB 107 IC bridge rectifier. The output power of the TENG can be utilized for continuously driving LEDs.

Further, the study was carried out to find the effect of triboelectric layer size (device size) on the TENG performance. Figure 7(a) shows the TENG response against hand tapping for different device dimensions of

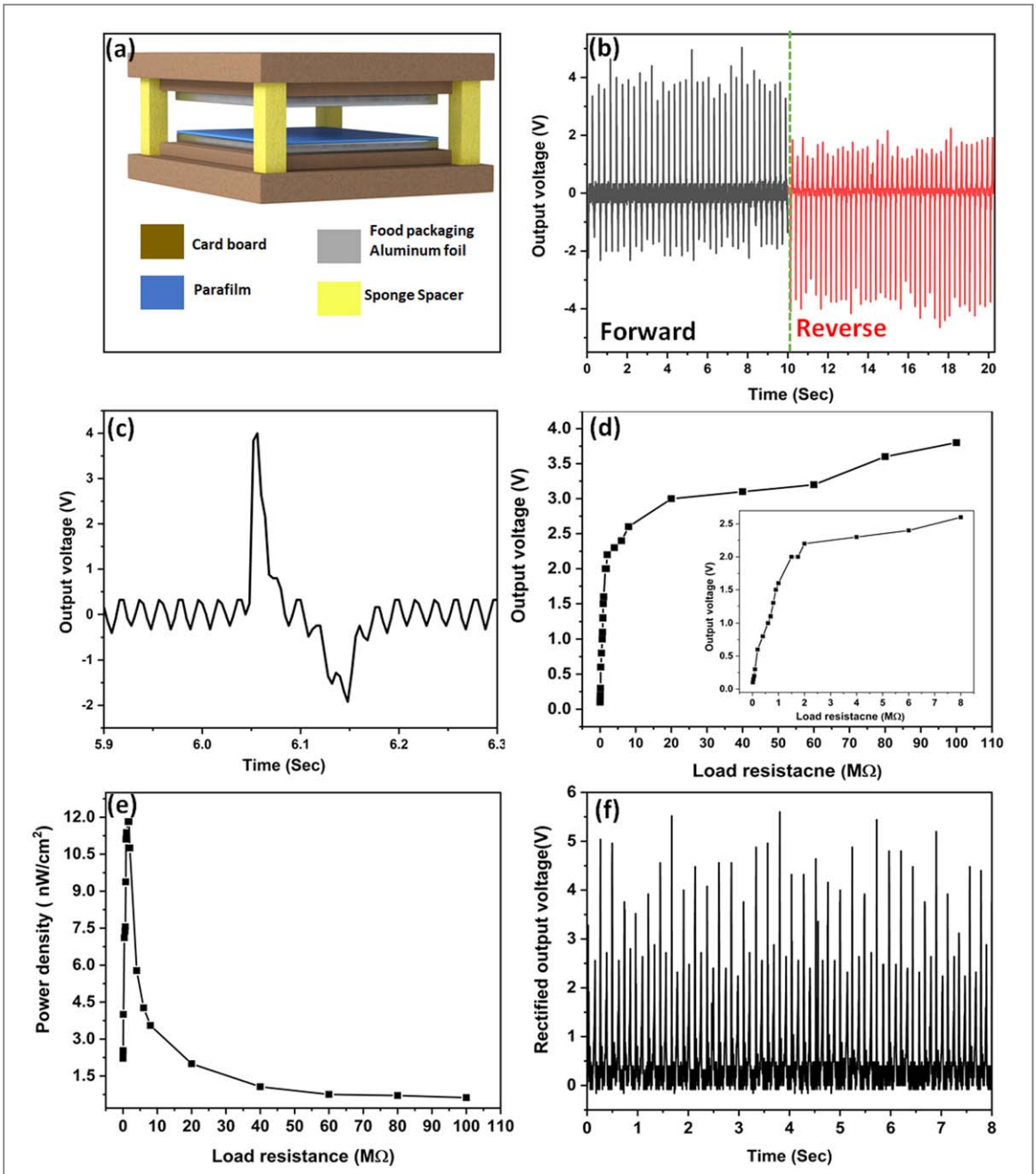

Figure 6. (a) Schematic of the TENG, (b) electric output of a TENG under forward and reverse connections, (c) a zoomed-in view of output voltage generated by TENG during a single cycle of operation, (d) output voltage as a function of the load resistance, (e) output power density as a function of the load resistance, (f) rectified output voltage of the TENG.

$5 \times 5, 8 \times 8, 15 \times 15\ cm^2$ for a separation distance of 1.5 cm. The averaged voltage values were obtained as 0.61 V ($5 \times 5\ cm^2$), 1.28 V ($8 \times 8\ cm^2$), and 3.96 V ($15 \times 15\ cm^2$). The enhancement in the output voltage from 0.61 V to 3.96 V was observed. This enhancement is due to the increased contact area of the triboelectric layers. Similar behaviour was reported for TENG's in earlier literature also [34, 43]. Figure 7(b) shows the TENG's output voltage characteristics under different tapping frequencies of 1, 2, 3, 5, and 6 Hz for a separation distance of 1.5 cm. It is evident from figure 7(b) that the output voltage was gradually increased with an increase in tapping frequency. This enhancement in the output voltage is attributed to the imperfect neutralization of accumulated residual charges due to rapid external tapping cycles, resulting in the increasing of triboelectric potential [7, 44–46]. At each frequency, the averaged voltage values were obtained as 0.5 V (1 Hz), 1 V (2 Hz), 2.2 V (3 Hz), 3 V (5 Hz), and 3.7 V (6 Hz).

Further, TENG performance was evaluated at the different spacing between the tribo-layers of 0.5 cm, 1.5 cm, and 2.5 cm with the help of a sponge. Figure 7(c) shows the TENG's output voltage variation under the same frequency of hand tapping with different spacing. TENG output voltage was increased with an increase in spacing between the tribo-layers. The open-circuit output voltage V_{oc} of TENG can be approximately expressed

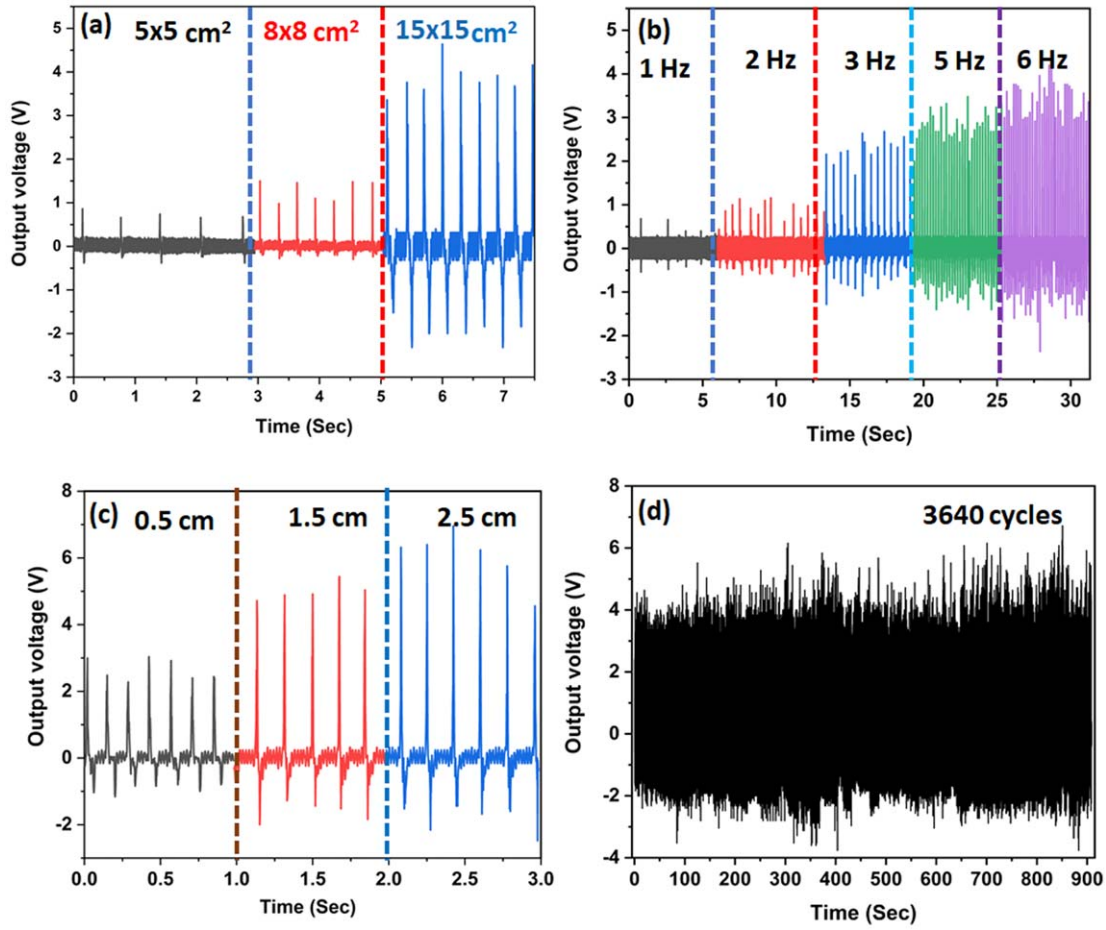

Figure 7. TENG output voltage as a function of (a) different area, (b) different frequency, (c) different spacing between parafilm and Aluminium, (d) output stability of the TENG under 3640 cycles.

as $V_{oc} = \frac{\sigma d}{\epsilon}$, where d is interlayer spacing, σ is the triboelectric charge density on the surface, and ε is the vacuum permittivity [8, 47]. According to the open-circuit output voltage expression, the output voltage will increase with increasing the interlayer distance. Similar behaviour was observed for other TENG devices in the literature [34, 46, 47]. The stability and durability of the TENG are essential factors to ensuring its practical applications. The output voltage was measured under external hand tapping force for 3640 cycles to examine the TENG durability for long-term operation. Figure 7(d) shows that the generated voltage did not degrade after 3640 cycles, indicating the high stability of fabricated TENG. Further, TENG response was recorded at different time points, such as immediately after fabrication, one month, and three months. In all the cases, TENG exhibited a stable output response (See SI, S4).

Figures 8(a)–(b) represents the enlarged view of the stability graphs at different time points. An average voltage of ~4 V was observed throughout all cycles. The TENG's output voltage was plotted for every 100th cycle (ex: 100, 200, 300 etc) shown in figure 8(c). The TENG's output voltage shows an average value of 4 ± 0.5 V, and this deviation is due to variation of hand tapping force and frequency.

Figure 9(a) shows the charging characteristics of various rating commercial capacitors such as 1 μF, 2.2 μF, 10 μF, 47 μF, and 100 μF for 900 s. The energy stored by the 1 μF capacitor was used to power up portable electronic devices such as a digital watch, calculator, thermometer, and 85 LEDs, as shown in figures 9(b)–(e). Further, TENG can also power up 4 LEDs continuously with hand tapping shown in figure 9(f) (See SI videos S1, S2, S3).

The stored charge on these different load capacitors was obtained using the basic equation $Q = CV$. Figure 10(a) shows the stored charges as a function of time for various load capacitors. The capacitor with a small enough value of 1 μF store a small amount of charge and quickly reaches the saturation value. It is evident from the figure that storage capacity is increased with an increase of load capacitance value. The capacitor with a large enough value of 100 μF stored the maximum charges of 200 μC in a given time of 900 s. At a constant time duration of 600 s, 1 μF capacitor saturation voltage and maximum stored charge were 4.5 V and 4.5 μC. In the case of 100 μF capacitor, the output voltage equals 2.3 V while the stored charges reach a maximum value of

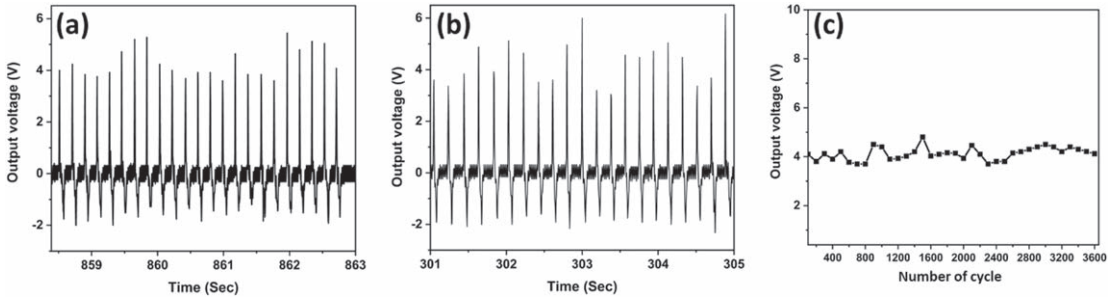

Figure 8. (a)–(b) Enlarged view of few cycles from the 3640 cycles (c) Output voltage values at every 100 cycles from the stability graph.

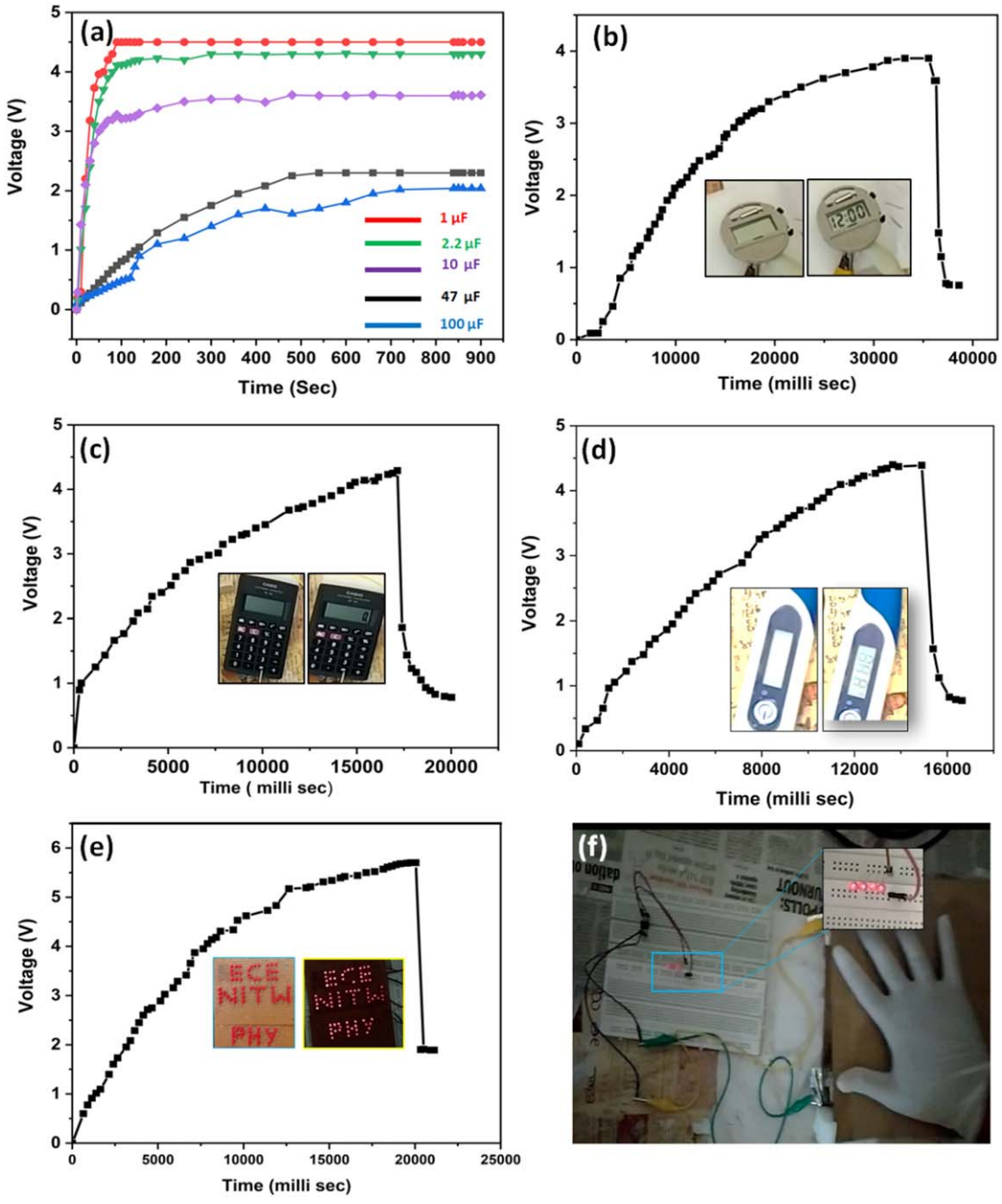

Figure 9. (a) Charging curves of different capacitors, charging and discharging behaviour of capacitor before and after power up the electronic devices (b) digital watch, (c) calculator, (d) thermometer and (e) 85 red LEDs, (f) image of the continuous powering on 4 LEDs under cyclic application of force.

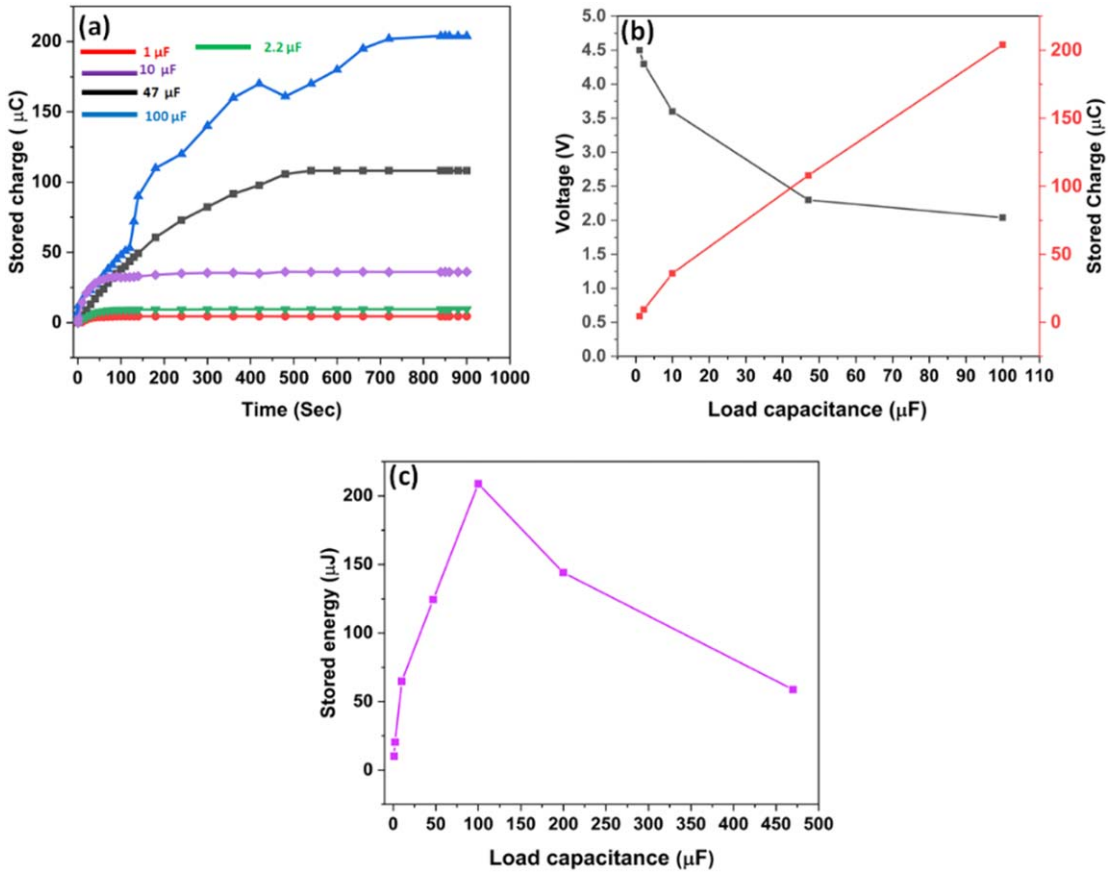

Figure 10. (a) Stored charge as a function of time for different load capacitors (b) The behaviour of output voltage and stored charges as a function of load capacitance (C_L) (c) The stored energy as a function of C_L.

204 μC. The output voltage and stored charge characteristics were analysed as a function of different load capacitance values shown in figure 10(b). There is an inversion relation between voltage and stored charges against corresponding C_L. Figure 10(c) shows the variation of maximum stored energy as a function of load capacitance. The maximum stored energy of 208.8 μJ was observed at the optimum C_L of 100 μF.

4. Conclusions

In summary, a new TENG has been demonstrated based on the waste food packaging Aluminium covers foil and the parafilm to power portable electronic devices. In our design, the parafilm and conducting side of WFPAC foil serve as the triboelectric pair. TENG's open-circuit voltage can reach ~4 V and the maximum power density 11.8 nW cm^{-2}. The prepared TENG was demonstrated to power up portable electronic devices and LEDs. The present work opens up a new triboelectric pair for energy harvesting. This new parafilm tribo-layer can form new triboelectric pairs with other materials for enhanced mechanical energy harvesting. Furthermore, the idea of using WFPAC foil reduces environmental pollution to a certain extent.

Data availability statement

All data that support the findings of this study are included within the article (and any supplementary files).

Declarations

Funding

Not applicable

Conflicts of interest/competing interests

The authors declare that they have no known competing financial interests.

ORCID iDs

P Ravi Sankar https://orcid.org/0000-0001-5652-0759
K Prakash https://orcid.org/0000-0001-9009-7325
P Supraja https://orcid.org/0000-0001-5612-4035
R Rakesh Kumar https://orcid.org/0000-0003-4023-9051
Siju Mishra https://orcid.org/0000-0003-3774-4196
D Haranath https://orcid.org/0000-0002-7936-6165

References

[1] Mathew A A, Chandrasekhar A and Vivekanandan S 2021 A review on real-time implantable and wearable health monitoring sensors based on triboelectric nanogenerator approach *Nano Energy* **80** 105566
[2] Kim W-G, Kim D-W, Tcho I-W, Kim J-K, Kim M-S and Choi Y-K 2021 Triboelectric nanogenerator: structure, mechanism, and applications *ACS Nano* **15** 258–87
[3] Cui N, Liu J, Gu L, Bai S, Chen X and Qin Y 2015 Wearable triboelectric generator for powering the portable electronic devices *ACS Appl. Mater. Interfaces* **7** 18225–30
[4] Zhu J, Zhu P, Yang Q, Chen T, Wang J and Li J 2020 A fully stretchable textile-based triboelectric nanogenerator for human motion monitoring *Mater. Lett.* **280** 128568
[5] Zhou Y, Shen M, Cui X, Shao Y, Li L and Zhang Y 2021 Triboelectric nanogenerator based self-powered sensor for artificial intelligence *Nano Energy* **84** 105887
[6] Ahmed A, Hassan I, El-Kady M F, Radhi A, Jeong C K, Selvaganapathy P R, Zu J, Ren S, Wang Q and Kaner R B 2019 Integrated triboelectric nanogenerators in the era of the internet of things *Adv. Sci.* **6** 1802230
[7] Fan F R, Tian Z Q and Lin Wang Z 2012 Flexible triboelectric generator *Nano Energy* **1** 328–34
[8] Niu S and Wang Z L 2015 Theoretical systems of triboelectric nanogenerators *Nano Energy* **14** 161–92
[9] Niu S, Wang S, Lin L, Liu Y, Zhou Y S, Hu Y and Wang Z L 2013 Theoretical study of contact-mode triboelectric nanogenerators as an effective power source *Energy Environ. Sci.* **6** 3576–83
[10] Mallineni S S K, Behlow H, Dong Y, Bhattacharya S, Rao A M and Podila R 2017 Facile and robust triboelectric nanogenerators assembled using off-the-shelf materials *Nano Energy* **35** 263–70
[11] Huang T, Lu M, Yu H, Zhang Q, Wang H and Zhu M 2015 Enhanced power output of a triboelectric nanogenerator composed of electrospun nanofiber mats doped with graphene oxide *Sci Rep.* **5** 1–8
[12] Wu C, Wang A C, Ding W, Guo H and Wang Z L 2019 Triboelectric nanogenerator: a foundation of the energy for the new era *Adv. Energy Mater.* **9** 1–25
[13] Lin Z, Chen J and Yang J 2016 Recent progress in triboelectric nanogenerators as a renewable and sustainable power source *J. Nanomater.* **2016** 1–24
[14] Yang B, Zeng W, Peng Z H, Liu S R, Chen K and Tao X M 2016 A fully verified theoretical analysis of contact-mode triboelectric nanogenerators as a wearable power source *Adv. Energy Mater.* **6** 1–8
[15] Shao J, Willatzen M and Wang Z L 2020 Theoretical modeling of triboelectric nanogenerators (TENGs) *J. Appl. Phys.* **128** 111101–32
[16] Zhou L, Liu D, Wang J and Wang Z L 2020 Triboelectric nanogenerators: fundamental physics and potential applications *Friction* **8** 481–506
[17] Luo J and Wang Z L 2020 Recent progress of triboelectric nanogenerators: from fundamental theory to practical applications *EcoMat* **2** 1–22
[18] Kim D W, Lee J H, Kim J K and Jeong U 2020 Material aspects of triboelectric energy generation and sensors *NPG Asia Mater.* **12** 6
[19] Zhang R and Olin H 2020 Material choices for triboelectric nanogenerators: a critical review *EcoMat* **2** 1–13
[20] Wang A C, Wu C, Pisignano D, Wang Z L and Persano L 2018 Polymer nanogenerators: opportunities and challenges for large-scale applications *J. Appl. Polym. Sci.* **135** 1–17
[21] Hu Y and Zheng Z 2019 Progress in textile-based triboelectric nanogenerators for smart fabrics *Nano Energy* **56** 16–24
[22] Chao S, Ouyang H, Jiang D, Fan Y and Li Z 2021 Triboelectric nanogenerator based on degradable materials *EcoMat* **3** 1–19
[23] Yu D, Zheng Z, Liu J, Xiao H, Huangfu G and Guo Y 2021 Superflexible and lead-free piezoelectric nanogenerator as a highly sensitive self-powered sensor for human motion monitoring *Nano-Micro Lett.* **13** 117
[24] Shaukat R A, Saqib Q M, Khan M U, Chougale M Y and Bae J 2021 Bio-waste sunflower husks powder based recycled triboelectric nanogenerator for energy harvesting *Energy Reports* **7** 724–31
[25] Wu J M, Chang C K and Chang Y T 2016 High-output current density of the triboelectric nanogenerator made from recycling rice husks *Nano Energy* **19** 39–47
[26] Xia K, Zhu Z, Fu J, Li Y, Chi Y, Zhang H, Du C and Xu Z 2019 A triboelectric nanogenerator based on waste tea leaves and packaging bags for powering electronic office supplies and behavior monitoring *Nano Energy* **60** 61–71
[27] Zhou Z *et al* 2018 Wireless self-powered sensor networks driven by triboelectric nanogenerator for *in situ* real time survey of environmental monitoring *Nano Energy* **53** 501–7
[28] Li Y, Zhao Z, Gao Y, Li S, Zhou L, Wang J and Wang Z L 2021 Low-cost, environmentally friendly, and high-performance triboelectric nanogenerator based on a common waste material *ACS Appl. Mater. Interfaces* **13** 30776–84
[29] Kaur J, Sawhney R S, Singh H and Singh M 2020 Electricity nanogenerator from egg shell membrane: a natural waste bioproduct *Int. J. Green Energy* **17** 309–18
[30] Zhang P, Zhang W and Zhang H 2021 A triboelectric nanogenerator based on waste polyvinyl chloride for Morse code generator *Sensors Actuators A Phys.* **322** 112633

[31] Han G, Wu B and Pu Y 2020 A triboelectric nanogenerator based on waste plastic bags for flexible vertical interconnection system *Microsyst. Technol.* **26** 3893–9
[32] Zhang J H, Li Y, Du J, Hao X and Huang H 2019 A high-power wearable triboelectric nanogenerator prepared from self-assembled electrospun poly(vinylidene fluoride) fibers with a heart-like structure *J. Mater. Chem.* A **7** 11724–33
[33] Zhang J, Fang Z, Shu C, Zhang J, Zhang Q and Li C 2017 A rotational piezoelectric energy harvester for efficient wind energy harvesting *Sensors Actuators A Phys.* **262** 123–9
[34] Wang Q, Chen M, Li W, Li Z, Chen Y and Zhai Y 2017 Size effect on the output of a miniaturized triboelectric nanogenerator based on superimposed electrode layers *Nano Energy* **41** 128–38
[35] Fan F R, Luo J, Tang W, Li C, Zhang C, Tian Z and Wang Z L 2014 Highly transparent and flexible triboelectric nanogenerators: performance improvements and fundamental mechanisms *J. Mater. Chem.* A **2** 13219–25
[36] Han Y, Han Y, Zhang X, Li L, Zhang C, Liu J, Lu G, Yu H-D and Huang W 2020 Fish gelatin based triboelectric nanogenerator for harvesting biomechanical energy and self-powered sensing of human physiological signals *ACS Appl. Mater. Interfaces* **12** 16442–50
[37] Xia K, Zhu Z, Zhang H and Xu Z 2018 A triboelectric nanogenerator as self-powered temperature sensor based on PVDF and PTFE *Appl. Phys. A Mater. Sci. Process.* **124** 1–7
[38] Niu S, Liu Y, Zhou Y S, Wang S, Lin L and Wang Z L 2015 Optimization of triboelectric nanogenerator charging systems for efficient energy harvesting and storage *IEEE Trans. Electron. Devices* **62** 641–7
[39] Niu S and Wang Z L 2014 Theoretical systems of triboelectric nanogenerators *Nano Energy* **14** 161–92
[40] Niu S, Zhou Y S, Wang S, Liu Y, Lin L, Bando Y and Wang Z L 2014 Simulation method for optimizing the performance of an integrated triboelectric nanogenerator energy harvesting system *Nano Energy* **8** 150–6
[41] Bird J 2017 *Electrical Circuit Theory and Technology* 6th edn (Newyork: Routledge)
[42] Bai Z, Xu Y, Li J, Zhu J, Gao C, Zhang Y, Wang J and Guo J 2020 An eco-friendly porous nanocomposite fabric-based triboelectric nanogenerator for efficient energy harvesting and motion sensing *ACS Appl. Mater. Interfaces* **12** 42880–90
[43] Kamilya T, Sarkar P K and Acharya S 2019 Unveiling peritoneum membrane for a robust triboelectric nanogenerator *ACS Omega* **4** 17684–90
[44] Ko Y H, Nagaraju G, Lee S H and Yu J S 2014 PDMS-based triboelectric and transparent nanogenerators with ZnO nanorod arrays *ACS Appl. Mater. Interfaces* **6** 6631–7
[45] Li W, Sun J and Chen M 2014 Triboelectric nanogenerator using nano-Ag ink as electrode material *Nano Energy* **3** 95–101
[46] Pan R, Xuan W, Chen J, Dong S, Jin H, Wang X, Li H and Luo J 2018 Fully biodegradable triboelectric nanogenerators based on electrospun polylactic acid and nanostructured gelatin films *Nano Energy* **45** 193–202
[47] Hou T C, Yang Y, Zhang H, Chen J, Chen L J and Lin Wang Z 2013 Triboelectric nanogenerator built inside shoe insole for harvesting walking energy *Nano Energy* **2** 856–62